

# Functional photoreceptor loss revealed with adaptive optics: An alternate cause of color blindness

Joseph Carroll\*<sup>†</sup>, Maureen Neitz\*<sup>‡§</sup>, Heidi Hofer\*, Jay Neitz\*<sup>‡§</sup>, and David R. Williams\*

\*Center for Visual Science, University of Rochester, Rochester, NY 14627-0270; and Departments of <sup>‡</sup>Ophthalmology and <sup>§</sup>Cell Biology, Neurobiology, and Anatomy, Medical College of Wisconsin, Milwaukee, WI 53226

Edited by Jeremy Nathans, Johns Hopkins University School of Medicine, Baltimore, MD, and approved March 16, 2004 (received for review March 1, 2004)

**There is enormous variation in the X-linked L/M (long/middle wavelength sensitive) gene array underlying “normal” color vision in humans. This variability has been shown to underlie individual variation in color matching behavior. Recently, red–green color blindness has also been shown to be associated with distinctly different genotypes. This has opened the possibility that there may be important phenotypic differences within classically defined groups of color blind individuals. Here, adaptive optics retinal imaging has revealed a mechanism for producing dichromatic color vision in which the expression of a mutant cone photopigment gene leads to the loss of the entire corresponding class of cone photoreceptor cells. Previously, the theory that common forms of inherited color blindness could be caused by the loss of photoreceptor cells had been discounted. We confirm that remarkably, this loss of one-third of the cones does not impair any aspect of vision other than color.**

cone mosaic | dichromacy | retinal imaging

Human trichromacy relies on three different cone types in the retina; long- (L), middle- (M), and short- (S) wavelength-sensitive. Dichromatic color vision results from the functional loss of one cone class; however, one of the central questions has been whether individuals with this form of red–green color blindness have lost one population of cones or whether they have normal numbers of cones filled with either of two instead of three pigments. Evidence has accumulated favoring the latter view, in which the photopigment in one class of cone is replaced, but the issue has not been resolved directly. Berendschot *et al.* (1) measured optical reflectance spectra of the fovea for normals and dichromats, and their analysis favored a replacement model. Psychophysical experiments, based on frequency of seeing curves, have also provided evidence that the packing of foveal cones in dichromats is comparable to that in trichromats (2, 3). Most recently, in comparing mean contrast gains derived from the electroretinogram (ERG) for dichromats to those of trichromats, Kremers *et al.* (4) concluded that complete replacement occurs in dichromacy.

The L- and M-cone photopigments are encoded by genes that reside in a head-to-tail tandem array on the X chromosome (5). Two categories of mutations of these genes have been found to be associated with dichromacy. In one category of mutations, the gene(s) for a spectral class of pigment have been deleted or replaced with a functional gene for a different spectral class (6–10). In the other genetic category, a normal gene is replaced by a mutant one encoding a photopigment that does not function properly (11, 12). The most frequently reported example of this latter cause is a mutation that substitutes the amino acid arginine for a cysteine at position 203 (C203R) of the pigment molecule. This cysteine is highly conserved among all G protein-coupled receptors, and is involved in forming an essential disulfide bond in the photopigment molecule (13). The mutation was originally discovered in association with blue cone monochromacy (14) and, when present, renders the pigment nonfunctional (15). Given the two different genotypic categories of dichromats, the purpose of the experiments described here was to explore the

possibility that they are associated with different phenotypes within what has classically been supposed to be a single class of dichromat.

Adaptive optics enables visualization of cone photoreceptors with unprecedented resolution by correcting for the eye’s aberrations (16). When combined with retinal densitometry, the spectral identity of individual cones can be deduced and pseudo-color images of the trichromatic cone mosaic in the living human eye can be obtained (17). Here, we used this technique to obtain images of the cone mosaic in two individuals who represent the two different classes of genetic defect in dichromats. In a person in whom the L gene was replaced by one encoding an M photopigment, the L cones were replaced by M cones and he, thus, had a normal number of functional cones in the central retina. The results for this person confirm that complete replacement of a cone class can occur, as had been suggested by the studies reviewed above. However, in contrast, in an individual in whom the normal M-pigment gene was replaced by one that encodes a nonfunctional pigment, patchy loss of normal cones throughout the photoreceptor mosaic was observed. In this person, color blindness is associated with a normal mosaic of L and S cones; however, there were dark patches where his normal M cones would have been.

## Materials and Methods

**Subjects.** All subjects provided informed consent after the nature and possible consequences of the study were explained. All research followed the tenets of the Declaration of Helsinki, and study protocols were approved by the institutional research boards at the Medical College of Wisconsin (genetics, color vision testing, and electroretinography) and the University of Rochester (adaptive optics imaging). Two dichromats (NC, age 26, and MM, age 32) and one trichromat (JP, age 28) were recruited for this study. Corrected visual acuity for NC was 20/16, MM and JP were 20/20 uncorrected. A complete ophthalmic examination including visual acuity measurement, slit lamp examination, and dilated funduscopic examination was performed on all subjects. Color vision was assessed by using a variety of tests, including the Rayleigh match, pseudoisochromatic plates (AO-HRR, Dvorine, and Ishihara) and the Neitz Test of Color Vision (18).

**Molecular Genetics.** DNA was extracted from whole blood obtained from all three subjects (19) and used in a previously described real-time quantitative PCR assay to estimate the relative number of L and M genes in the X-chromosome visual pigment gene array (18). The L and M genes were selectively amplified by long-distance PCR, and the product obtained was subsequently used to amplify separately exons 2, 3, and 4 of L and of M genes for direct DNA sequence analysis. The primers and

This paper was submitted directly (Track II) to the PNAS office.

Abbreviations: ERG, electroretinogram; S, short wavelength sensitive; M, middle wavelength sensitive; L, long wavelength sensitive.

<sup>†</sup>To whom correspondence should be addressed. E-mail: jcarroll@cvs.rochester.edu.

© 2004 by The National Academy of Sciences of the USA

thermal cycling parameters for all amplifications were reported (20). The resultant PCR products were directly sequenced with the AmpliTaq FS sequencing kit (Applied Biosystems), and sequencing analysis was done with the ABI 310 genetic analyzer.

**Flicker-Photometric ERG.** Details on signal processing and the procedure and apparatus to record the electroretinogram have been published (20, 21). Fiber from the DTL Plus electrode was used as the active corneal electrode. A test and a reference beam were presented in Maxwellian view and superimposed to illuminate an area of retina subtending  $\approx 70^\circ$ . High-speed electromagnetic shutters were used to alternately present the reference and test lights at 31.25 Hz. Spectral sensitivity was determined by adjusting the intensity of the test light [whose wavelength was controlled by a Varispec (Cambridge Research and Instrumentation, Cambridge, MA) liquid-crystal electronically tunable filter] until the ERG signal it produced exactly matched that produced by the fixed-intensity reference light. Spectral sensitivity data were best fit to a vitamin-A<sub>1</sub> visual pigment template by allowing the  $\lambda_{\max}$  to vary (20).

**High-Resolution Retinal Imaging.** Imaging was done by using the Rochester Second Generation Adaptive Optics System (see ref. 22 for a schematic and system details). The head was stabilized by using a dental impression on a bite bar. The subjects' right eye was dilated and accommodation suspended through use of a combination of Phenylephrine Hydrochloride (2.5%) and Tropicamide (1%). In a continuous closed-loop fashion, we measured the eye's monochromatic aberrations over a 6.8-mm pupil with a Shack-Hartmann wavefront sensor and corrected for them with a 97-channel deformable mirror (Xinetics, Devins, MA) until the root mean square wavefront error fell below 0.1  $\mu\text{m}$  or 800 ms had elapsed, whichever happened first. Additional details on wavefront measurement and compensation have been published (16, 22, 23). Once a wavefront correction was obtained, a retinal image was acquired by illuminating the retina with a 1° diameter, 4-ms flash [550 nm, 25-nm bandwidth (full width at half max)] from a krypton arc flash lamp. The short duration of the flash helped to minimize the effects of motion blur on the accompanying retinal image. Images were taken with a cooled charge-coupled device (CCD) camera (Roper Scientific, Trenton, NJ). To avoid possible edge artifacts from the deformable mirror, imaging was done over a 6-mm pupil. A circular fixation target was used to record the relative retinal location of each image (i.e., nasal, temporal, superior, or inferior as well as eccentricity). Images were obtained over a 2- to 3-day period and averaged (using a MATLAB-based image registration algorithm; MathWorks, Natick, MA) to minimize the effect of variability in cone reflectance over time (23).

**Spatially Localized Retinal Densitometry.** To identify cone subtypes *in vivo*, we combined retinal densitometry with our high-resolution retinal imaging paradigm described above. Details on the procedure to classify individual cones as S, M, or L have been published (17, 24), only a brief outline is given here. Individual cones in the retinal mosaic were classified by comparing images taken when all of the photopigment was bleached with those taken when it was fully regenerated or when one class of photopigment was selectively bleached with either a 470- or 650-nm light. Once the S cones were identified and removed from subsequent analysis, the remaining cones could be identified as M or L by plotting the absorbance of each cone after the 650-nm bleach vs. that after the 470-nm bleach. Here, absorbance is defined as 1 minus the ratio of the selectively bleached image to the corresponding fully bleached image. Bleaching levels were set to maximize the difference in photopigment concentration between the L- and M-cone classes (and thus optimize our chances of distinguishing them from one

another), based on knowledge of the L and M spectral sensitivity curves as well as photopigment kinetics (25, 26). Bleaching levels were  $\approx 25 \times 10^6$  Troland-seconds for the 550-nm full bleach,  $\approx 7.7 \times 10^6$  Troland-seconds for the 650-nm bleach, and  $\approx 5.2 \times 10^6$  Troland-seconds for the 470-nm bleach.

**Procedure for Estimating Cone Density.** Average images from each retinal location were imported into a graphics program (PHOTOSHOP, Adobe Systems, Mountain View, CA) and merged together to form a single montage of the central retina for analysis. A freely available image-processing program (IMAGEJ, National Institutes of Health) was used to manually identify the cones in each subject's montage. The (x, y) coordinates of the cones were stored in a text array and cone density was estimated by using a custom MATLAB algorithm. The list of cone coordinates was scanned by a sampling window with a radius of 20.6  $\mu\text{m}$  (the position of the sampling window was incremented/decremented by multiples of the window radius). At each location, the number of cones within the sampling window was recorded. The foveal center was taken to be the region of highest cone density in each subjects' montage. The area of retina sampled at each point was that used by Curcio *et al.* (27),  $\approx 1,300 \mu\text{m}^2$  (average visual angle equivalent is 0.14° diameter). Source code for the cone-density algorithm is available upon request.

## Results

**Color Vision and Ophthalmic Examination.** Color vision was classified in three males based on color matching performance on an anomaloscope (the Rayleigh match). This procedure requires the subject to match a spectral yellow light to an adjacent mixture of spectral red and green lights. JP was classified as a normal trichromat, making a match over a narrow range of red/green mixtures. Both MM and NC were able to make a Rayleigh match by adjusting the intensity of the monochromatic yellow light, regardless of the red/green mixture ratio. This behavior is indicative of the presence of a single photopigment in the middle-to-long wavelength region of the spectrum (i.e., dichromacy). MM showed a typical protanopic luminosity loss for long wavelengths, whereas NC kept the luminance of the yellow light approximately equal when matching either primary and all red/green mixtures, consistent with a deuteranopic phenotype.

Ophthalmic exams on MM and JP were completely normal. NC had 2.5 diopters of myopia OU. Slit lamp examination of NC was unremarkable, and visual fields were also normal. Dilated fundus examination revealed a temporal crescent of retinal pigment epithelium (RPE) atrophy consistent with myopia and slight retinal vascular attenuation OU. There was no disk pallor or edema, and the cup-to-disk ratio was 0.3 OD and 0.4 OS, which is within normal limits (28). There was trace RPE pigment irregularity in the fovea OU, which was considered within normal limits. Fluorescein angiography demonstrated normal vascular filling with no evidence of hyperfluorescence or hypofluorescence.

**L/M Gene Arrangement in Dichromats.** The X-linked photopigment gene(s) of NC and MM were analyzed by using previously described techniques (20). Both have two genes on their X-chromosome. MM is an example in which the L-pigment gene has been replaced by a gene encoding an M pigment, both the first and second gene in his array encode M pigments. In contrast, NC is an example in which a normal M-pigment gene has been replaced by a gene encoding a nonfunctional pigment. For NC, sequencing of the spectral tuning sites indicates that one gene should encode a normal L and the other a normal M pigment. However, at nonspectral tuning sites, his M-pigment gene encodes a combination of amino acids that has not been observed in normally functioning L or M pigments. It has been observed in five other unrelated families, every time associated with the

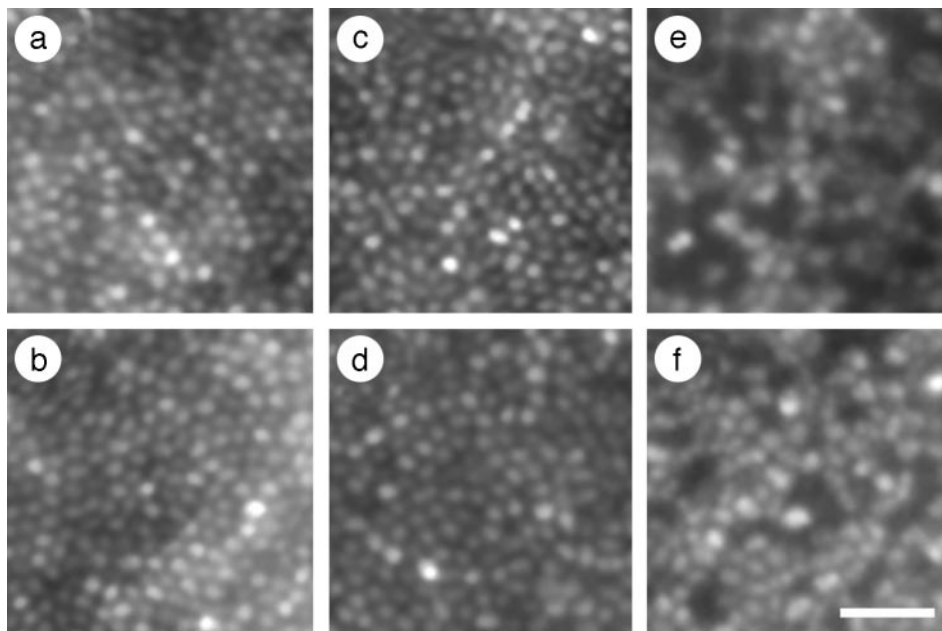


**Fig. 1.** Retinal images from the right eyes of a trichromat and two dichromats. JP (age 28) is a trichromat, MM (age 32) is a protanope, and NC (age 26) is a deuteranope. Images are at  $\approx 1^\circ$  eccentricity from nasal (a, c, and e) or temporal (b, d, and f) retina. MM (c and d) was classified as a protanope, and NC (e and f) was classified as a deuteranope based on Rayleigh match data and performance on standard color vision tests. Images from trichromat JP (a and b) are shown for comparison. (Scale bar, 20  $\mu\text{m}$ .)

loss of function of the corresponding cone class (data not shown, see ref. 10 for discussion). Just as the C203R folding mutation renders the pigment nonfunctional, we propose that this mutant pigment does not function properly.

**Retinal Imaging in Dichromats.** Retinal images were obtained by using the Rochester Second Generation Adaptive Optics System (22). Fig. 1 shows retinal images from trichromat JP and both dichromats. The mosaic of one dichromat, MM (Fig. 1 c and d), is indistinguishable from that of the trichromat (Fig. 1 a and b), whereas the mosaic of the other dichromat, NC (Fig. 1 e and f), contains numerous dark regions. The complete cone mosaics of JP and MM are typical of other trichromats tested in the lab. For NC, images from 33 different retinal locations were merged together into a single montage, illustrating that the dark regions are ubiquitous throughout his central retina (see Fig. 5, which is published as supporting information on the PNAS web site). Based on the evidence below, we hypothesize that these regions contained cones that expressed a mutant M pigment and were either severely damaged or lost.

**Loss of M-Cone Function in NC.** Besides NC's behavior in color matching, there are two additional sources of evidence for complete loss of his M-cone function. First, none of the cones identified in NC's retina appear to contain M pigment. In trichromats, after the S cones have been identified, the absorbance values for single cones after 470-nm and 650-nm bleaches produce a clear bimodal distribution (17), which represents the L- and the M-cone classes (see Fig. 2 c and d for data from trichromat JP). Previous data on MM (a protanope) revealed only a single mode after a similar analysis (17). Fig. 2 a and b shows absorbances from nearly 1,000 cones in NC's retina. As with MM, only a single mode is revealed, indicating the presence of a single L/M cone class. Second, NC's spectral sensitivity function (see Fig. 3) obtained by using the flicker-photometric ERG is indistinguishable from the spectral sensitivities of known deuteranope populations (29–31), and also from *in vitro* spectra for isolated L cones and L-cone pigment (32–34). Likewise,

MM's spectral sensitivity function is indistinguishable from the spectral sensitivities of known protanope populations (30, 35), and also from *in vitro* spectra for isolated M-cone pigment (32, 33). These data corroborate the anomaloscope findings that there is only a single functional L/M pigment in NC and MM.

**Modeling M-Cone Loss in NC.** To test the hypothesis that the dark regions contained M cones that were damaged or lost, we modeled the dark regions in the images by filling them with cones of approximately the same diameter and spacing as the visible cones in the image. A statistical test (24) indicated that the modeled M cones were randomly interleaved amongst the visible cones in the image, consistent with the random organization of the M- and L-cone submosaics (24, 36–38). Fig. 4 shows a pseudocolor image of NC's modeled retina. If the M cones in NC's retina were selectively lost, we would expect the ratio of visible:modeled cones to be comparable to normal L:M cone ratios (after removing the S cones). This ratio in NC's image is 2.4:1, which is near the average L:M ratio in the population (31). Nevertheless, there is large variability in L:M ratio among individuals with normal color vision (31, 39, 40), so we cannot rule out the possibility that some normal L cones that were adjacent to failing M cones have also been lost, thereby deflating the inferred ratio of visible:modeled cones. However, if significant loss of these L cones had occurred, the modeled cones would have appeared to be clumped instead of being randomly interleaved among the visible cones. Taken together, these data support the hypothesis that the dark regions in NC's cone mosaic result from a selective and complete loss of functioning M cones, rather than a more generalized cone dystrophy.

**Foveal Cone Density.** Despite the fact that NC has a reduced number of normal appearing cones, he does have a region of higher cone density corresponding to a normal fovea. Peak foveal densities (cones per  $\text{mm}^2$ ) were as follows: JP, 148,825; MM, 114,219; NC, 82,671. Although NC has a reduced peak cone density, the fraction of lost cones was uniform across the foveal region. We analyzed the density of modeled cones and added this

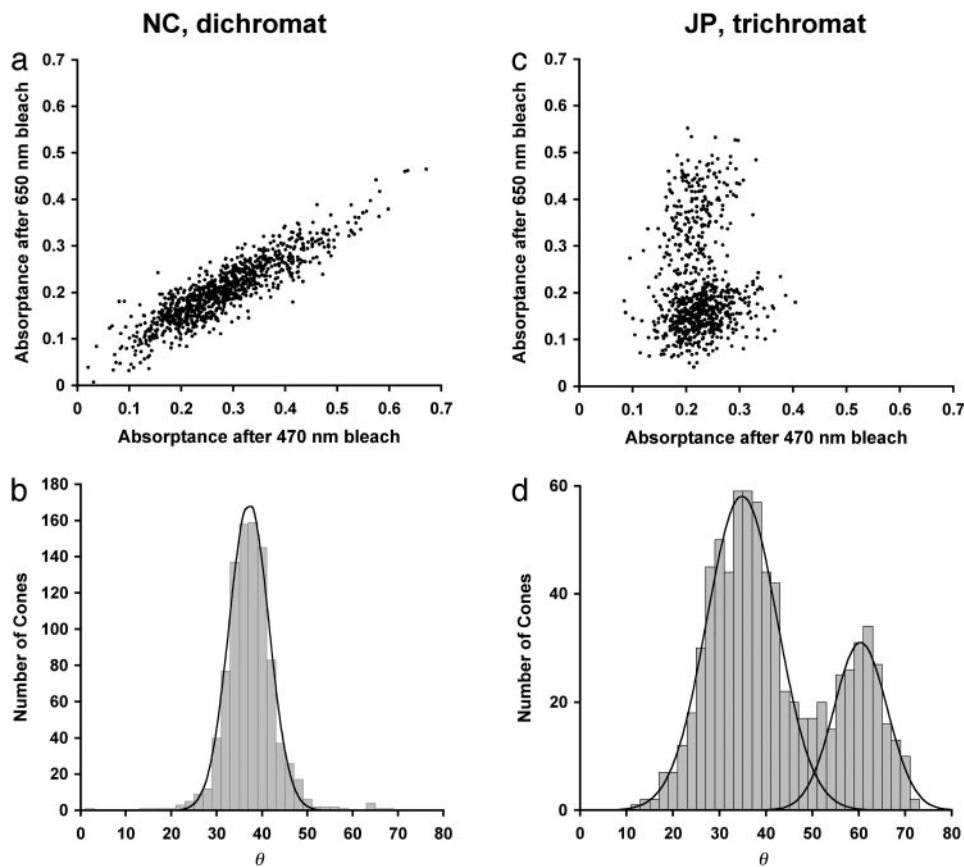


**Fig. 2.** Scatter plots and histograms of individual cone absorptances. (a) Scatter plot shows individual cone absorptances from NC's retinal images after the 470- and 650-nm selective bleaches. Cone absorptance was taken as the average value computed within a 0.4-arcmin square region centered on the cone. A total of 932 non-S cones in a 0.05-mm<sup>2</sup> area were analyzed (eccentricity of 0.5° temporal retina). (b) Histogram of individual cone absorptances, where the number of cones is plotted as a function of angle in the scatter plot in a. Solid line represents the best-fitting Gaussian curve ( $r^2 = 0.99$ ). The residual single mode is indicative of a single L/M cone type (17). (c) Same as in a, but for JP (trichromat). A total of 741 non-S cones in a 0.03-mm<sup>2</sup> area were analyzed (eccentricity of 1° temporal retina). L cones absorb relatively less after the 650-nm bleach and relatively more after the 470-nm bleach than the M cones do, thus they appear closer to the abscissa. (d) The histogram for JP. A sum of two Gaussian curves was fit to the histogram (solid lines,  $r^2 = 0.97$ ). The estimated L:M ratio from this analysis is 2.4:1.

value to the observed density of visible cones. The resulting value (118,746 cones per mm<sup>2</sup>) is consistent with that observed for the normal trichromat and the other dichromat, as well as published estimates of cone density in the human fovea (27, 41). Moreover, on a semilog plot, NC's cone density as a function of eccentricity has a slope parallel to that of MM and JP, as well as previous histological data (27) (data not shown). These data suggest that normal foveal migration of the cone photoreceptors (42, 43) occurred to a large extent in NC, and it was only after this that the M cones (lacking a functional cone photopigment) began to degenerate.

## Discussion

One of longest standing questions in color vision has been whether dichromacy results from loss of one cone class or replacement of the photopigment in one cone class by a pigment of a different spectral type. Here, adaptive optics imaging of the living retina has provided direct evidence that, although replacement occurs in some individuals, loss occurs in others. Based on the results reported here, we propose that loss of cone photoreceptors occurs when one of the first two genes in the X-chromosome array is substituted by a gene that encodes a nonfunctional pigment, and replacement of the photopigment in one cone class occurs when the first two genes encode the same class of functional photopigment. It is not

known what the cone mosaic looks like in dichromats who have only a single gene in their L/M array, although based on a current model of L/M gene expression (44), one might expect them to have a complete cone mosaic. From genetic analyses of dichromats (8, 10), we anticipate that ≈15% of red-green dichromats will have lost cones, as was observed for NC. Additional imaging of dichromats with different genetic causes of dichromacy is necessary to test this.

The fact that a loss of one-third of NC's cones does not manifest itself in any standard clinical test (20/16 corrected acuity and a normal ophthalmic examination) other than a color vision defect presumably explains why the existence of individuals with his type of dichromacy was not appreciated previously. Nevertheless, there are tests that could be done in a vision laboratory in which the absent photoreceptors would be manifest. For example, NC would be expected to show deficits in psychophysical metrics that measure thresholds for extremely small spots of light designed to illuminate only a few cones (2, 3). His incomplete mosaic would also be expected to provide reduced protection from aliasing effects at lower temporal frequencies because of an undersampling of the retinal image. However, the fact that NC shows no deficit other than a loss of color vision in clinical tests further demonstrates an impressive property of our visual system: it can sustain substantial random loss of sampling elements and still provide high visual acuity (45, 46).

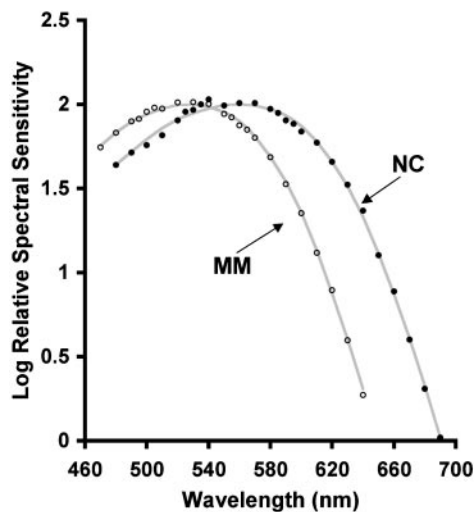


**Fig. 3.** Relative spectral sensitivity functions for MM and NC. Spectral sensitivity was measured with the flicker photometric ERG. Filled circles are from the right eye of NC, and open circles are from the right eye of MM. Solid lines represent vitamin-A<sub>1</sub> visual pigment templates with  $\lambda_{\max}$  values of 559 nm and 527 nm, consistent with typical deuteranope and protanope values, respectively (see text).

What are these dark regions? Cone photoreceptors can be seen in high-resolution retinal imaging *in vivo* because their waveguide properties cause the light reflected from them to be guided back toward the pupil center (47). Our ability to interpret what resides in the dark regions is limited; however, if NC has cone photoreceptors in these dark regions, they are incapable of reflecting light in a normal fashion. In retinitis pigmentosa (RP), expression of a mutant photopigment leads to primary rod cell death via apoptosis followed by death of neighboring cone photoreceptors (48, 49). We hypothesize that the cones that expressed the mutant M gene in NC's array have also died and previously resided in what are the dark regions in the image of his mosaic. If indeed the M cones have died, our analysis of the dark regions in NC's retinal image suggests that, unlike the rods and cones in RP, cones do not appear to be similarly dependent on each other, at least in this 26-year-old. However, there have been reports of generalized cone degeneration accompanying a congenital color vision defect (50–52), so it would be interesting to reexamine NC later in life.

Beyond the widespread loss of healthy waveguiding cones, we are left to wonder whether there are any postreceptoral changes in NC's visual system. Many of the dark regions in his cone mosaic are large enough to have nearly encompassed a midganglion cells' entire receptive field (53). This reduction (or complete loss) of input might have deleterious effects on the underlying ganglion cell, or it could result in synaptic reorganization where the ganglion cell simply draws from the remaining viable photoreceptors. There is evidence of a congenital photoreceptor abnormality leading to pronounced cortical changes in rod monochromats; Baseler *et al.* (54) showed that the absence (or near absence) of cone signals caused a central reorganization of the cortex in which cortical regions that normally respond to

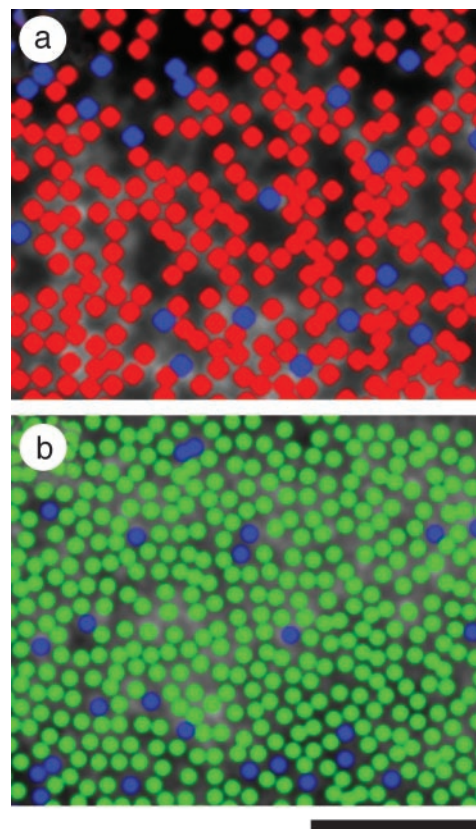


**Fig. 4.** Pseudocolor image of the dichromatic cone mosaic. Blue, green, and red colors represent the S, M, and L cones, respectively. (a) Subject NC's inferior retina at an eccentricity of 0.75°. All cones are of the S or L type (see text for details). (b) Subject MM's nasal retina at an eccentricity of 1°. All cones are of the S or M type, as indicated from previous results (17) as well as data presented here (see Fig. 3). (Scale bar, 50  $\mu\text{m}$ .)

signals from the all-cone foveola were found to respond robustly to rod-originated signals. This demonstration of a close relationship between congenital photoreceptor defects and brain development suggests that NC (who has lost more than one-third of his cones) might also show fundamental changes in his visual circuitry.

It is only with the introduction of adaptive optics imaging that these retinal features can be readily visualized. We anticipate that, for other visual disorders involving cone loss, adaptive optics imaging will enable much earlier detection and diagnosis and prove to be a valuable tool to detect retinal pathology that is otherwise invisible to current clinical methods.

We thank D. Gray, D. Han, J. Lin, G. Pan, J. Porter, and J. Wolfing for their assistance. We acknowledge financial support from the National Eye Institute (to J.C., M.N., J.N., and D.R.W.), Research to Prevent Blindness (to M.N. and D.R.W.) and the National Science Foundation (to H.H.). This work has been supported in part by the National Science Foundation Science and Technology Center for Adaptive Optics, managed by the University of California at Santa Cruz under Cooperative Agreement No. AST-9876783.

- Berendschot, T. T., van de Kraats, J. & van Norren, D. (1996) *J. Physiol.* **492**, 307–314.
- Cicerone, C. M. & Nerger, J. L. (1989) *Vision Res.* **29**, 1587–1595.
- Wesner, M. F., Pokorny, J., Shevell, S. K. & Smith, V. C. (1991) *Vision Res.* **31**, 1021–1037.
- Kremers, J., Usui, T., Scholl, H. P. N. & Sharpe, L. T. (1999) *Invest. Ophthalmol. Vis. Sci.* **40**, 920–930.

- Nathans, J., Thomas, D. & Hogness, D. S. (1986) *Science* **232**, 193–202.
- Nathans, J., Piantanida, T. P., Eddy, R. L., Shows, T. B. & Hogness, D. S. (1986) *Science* **232**, 203–210.
- Deeb, S. S., Lindsey, D. T., Hibiya, Y., Sanocki, E., Winderickx, J., Teller, D. Y. & Motulsky, A. G. (1992) *Am. J. Hum. Genet.* **51**, 687–700.
- Jagla, W. M., Jägle, H., Hayashi, T., Sharpe, L. T. & Deeb, S. S. (2002) *Hum. Mol. Genet.* **11**, 23–32.

9. Ueyama, H., Li, Y.-H., Fu, G.-L., Lertrit, P., Atchaneeyasakul, L., Oda, S., Tanabe, S., Nishida, Y., Yamade, S. & Ohkubo, I. (2003) *Proc. Natl. Acad. Sci. USA* **100**, 3357–3362.
10. Neitz, M., Carroll, J., Renner, A., Knau, H., Werner, J. S. & Neitz, J. (2004) *Vis. Neurosci.*, in press.
11. Winderickx, J., Sanocki, E., Lindsey, D. T., Teller, D. Y., Motulsky, A. G. & Deeb, S. S. (1992) *Nat. Genet.* **1**, 251–256.
12. Bollinger, K., Bialozynski, C., Neitz, J. & Neitz, M. (2001) *Color Res. Appl.* **26**, S100–S105.
13. Karnik, S. S., Sakmar, T. P., Chen, H.-B. & Khorana, H. G. (1988) *Proc. Natl. Acad. Sci. USA* **85**, 8459–8463.
14. Nathans, J., Davenport, C. M., Maumenee, I. H., Lewis, R. A., Hejtmancik, J. F., Litt, M., Lovrien, E., Welleber, R., Bachynski, B., Zwas, F., et al. (1989) *Science* **245**, 831–838.
15. Kazmi, M. A., Sakmar, T. P. & Ostrer, H. (1997) *Invest. Ophthalmol. Vis. Sci.* **38**, 1074–1081.
16. Liang, J., Williams, D. R. & Miller, D. (1997) *J. Opt. Soc. Am. A* **14**, 2882–2892.
17. Roorda, A. & Williams, D. R. (1999) *Nature* **397**, 520–522.
18. Neitz, M. & Neitz, J. (2001) *Color Res. Appl.* **26**, S239–S249.
19. Neitz, M., Neitz, J. & Grishok, A. (1995) *Vision Res.* **35**, 2395–2407.
20. Carroll, J., McMahon, C., Neitz, M. & Neitz, J. (2000) *J. Opt. Soc. Am. A* **17**, 499–509.
21. Jacobs, G. H., Neitz, J. & Krogh, K. (1996) *J. Opt. Soc. Am. A* **13**, 641–648.
22. Hofer, H., Chen, L., Yoon, G. Y., Singer, B., Yamauchi, Y. & Williams, D. R. (2001) *Opt. Express* **8**, 631–643.
23. Pallikaris, A., Williams, D. R. & Hofer, H. (2003) *Invest. Ophthalmol. Vis. Sci.* **44**, 4580–4592.
24. Roorda, A., Metha, A. B., Lennie, P. & Williams, D. R. (2001) *Vision Res.* **41**, 1291–1306.
25. Rushton, W. A. H. & Henry, G. H. (1968) *Vision Res.* **8**, 617–631.
26. Hollins, M. & Alpern, M. (1973) *J. Gen. Physiol.* **62**, 430–447.
27. Curcio, C. A., Sloan, K. R., Kalina, R. E. & Hendrickson, A. E. (1990) *J. Comp. Neurol.* **292**, 497–523.
28. Miglior, S., Brigatti, L., Velati, P., Balestreri, C., Rossetti, L., Bujtar, E. & Orzalesi, N. (1994) *Curr. Eye Res.* **13**, 119–124.
29. Jacobs, G. H. & Calderone, J. B. (1997) in *John Dalton's Colour Vision Legacy*, eds. Dickerson, C., Murray, I. & Carden, D. (Taylor & Francis, London), pp. 47–54.
30. Sharpe, L. T., Stockman, A., Jägle, H., Knau, H., Klausen, G., Reitner, A. & Nathans, J. (1998) *J. Neurosci.* **18**, 10053–10069.
31. Carroll, J., Neitz, M. & Neitz, J. (2002) *J. Vis.* **2**, 531–542.
32. Merbs, S. L. & Nathans, J. (1992) *Nature* **356**, 433–435.
33. Asenjo, A. B., Rim, J. & Oprian, D. D. (1994) *Neuron* **12**, 1131–1138.
34. Kraft, T. W., Neitz, J. & Neitz, M. (1998) *Vision Res.* **38**, 3663–3670.
35. Neitz, M., Neitz, J. & Jacobs, G. H. (1995) *Vision Res.* **35**, 2095–2103.
36. Mollon, J. D. & Bowmaker, J. K. (1992) *Nature* **360**, 677–679.
37. Packer, O. S., Williams, D. R. & Bensinger, D. G. (1996) *J. Neurosci.* **16**, 2251–2260.
38. Bowmaker, J. K., Parry, J. W. L. & Mollon, J. D. (2003) in *Normal & Defective Colour Vision*, eds. Mollon, J. D., Pokorny, J. & Knoblauch, K. (Oxford Univ. Press, New York), pp. 39–50.
39. Rushton, W. A. H. & Baker, H. D. (1964) *Vision Res.* **4**, 75–85.
40. Pokorny, J., Smith, V. C. & Wesner, M. F. (1991) in *From Pigments to Perception: Advances in Understanding Visual Processes*, eds. Valberg, A. & Lee, B. B. (Plenum, New York), pp. 23–34.
41. Williams, D. R. (1988) *Vision Res.* **28**, 433–454.
42. Hendrickson, A. E. & Yuodelis, C. (1984) *Ophthalmology* **91**, 603–612.
43. Yuodelis, C. & Hendrickson, A. (1986) *Vision Res.* **26**, 847–855.
44. Smallwood, P. M., Wang, Y. S. & Nathans, J. (2002) *Proc. Natl. Acad. Sci. USA* **99**, 1008–1011.
45. Williams, D. R. (1990) in *Advances in Photoreception: Proceedings of a Symposium on Frontiers of Visual Science* (Natl. Acad. Press, Washington, DC), pp. 135–148.
46. Geller, A. M. & Sieving, P. A. (1993) *Vision Res.* **33**, 1509–1524.
47. Miller, D. T., Williams, D. R., Morris, G. M. & Liang, J. (1996) *Vision Res.* **36**, 1067–1079.
48. Cideciyan, A. V., Hood, D. C., Huang, Y., Banin, E., Zong-Yi, L., Stone, E. M., Milam, A. H. & Jacobson, S. G. (1998) *Proc. Natl. Acad. Sci. USA* **95**, 7103–7108.
49. Milam, A. H., Li, Z. Y. & Fariss, R. N. (1998) *Prog. Retin. Eye Res.* **17**, 175–205.
50. Reichel, E., Bruce, A. M., Sandberg, M. A. & Berson, E. L. (1989) *Am. J. Ophthalmol.* **108**, 540–547.
51. Kellner, U., Sadowski, B., Zrenner, E. & Foerster, M. H. (1995) *Invest. Ophthalmol. Vis. Sci.* **36**, 2381–2387.
52. Scholl, H. P. N., Kremers, J. & Wissinger, B. (2001) *Curr. Eye Res.* **22**, 221–228.
53. Croner, L. J. & Kaplan, E. (1995) *Vision Res.* **35**, 7–24.
54. Baseler, H. A., Brewer, A. A., Sharpe, L. T., Morland, A. B., Jägle, H. & Wandell, B. A. (2002) *Nat. Neurosci.* **5**, 364–370.